PIER Photonics

(Received 6 July 2026, Accepted 25 July 2026, Scheduled 27 July 2026)

Record-high Third-order Optical Nonlinearity in 2D ITO via Quantum Confinement at Telecommunication Wavelengths

Zhuoer Chen[1, 2, 3, †], Yiyun Zhang[1, 2, 3, †], Junru Niu[1, 2, 3], Lian Shen[1, 2, 3], Yeon Ui Lee[4], Hongsheng Chen[1, 2, 3, *], Bingtao Gao[1, 2, 3, *], and Shilong Li[1, 2, 3, *]

[1] *State Key Laboratory of Extreme Photonics and Instrumentation*
ZJU-Hangzhou Global Scientific and Technological Innovation Center, Zhejiang University, Hangzhou 310027, China
[2] *The Electromagnetics Academy at Zhejiang University*
College of Information Science and Electronic Engineering, Zhejiang University, Hangzhou 310027, China
[3] *Zhejiang Key Laboratory of Intelligent Electromagnetic Control and Advanced Electronic Integration*
Jinhua Institute of Zhejiang University, Zhejiang University, Jinhua 321099, China
[4] *Department of Physics, Chungbuk National University, Cheongju, Chungbuk 28644, Republic of Korea*

ABSTRACT: All-optical nonlinear modulators, capable of femtosecond-scale signal modulation, are pivotal for high-speed data transmission in next-generation space optical communications. However, the inherently weak third-order optical nonlinearity of conventional materials remains a significant bottleneck for efficient nonlinear signal processing. In this work, we unveil the extraordinary third-order nonlinear susceptibility $\chi^{(3)}$ of atomically thin two-dimensional (2D) indium tin oxide (ITO) films within the 1550-nm telecommunications band. By leveraging quantum confinement effects, these 2D ITO layers form discrete electronic subbands that dramatically enhance intersubband transition dipole moments and thus the optical responses. Experimental measurements reveal a record-high angle-averaged $\chi^{(3)}$ value of 2.0×10^{-14} m^2/V^2, representing an approximately 300-fold enhancement over bulk ITO and surpassing graphene by a factor of five. Furthermore, the 2D ITO films maintain high transparency and possess the potential for ultrafast response speeds inherent to electronic nonlinear processes, making them ideal candidates for compact nonlinear photonic integration. These findings demonstrate that 2D ITO, as a representative example of bandgap-engineered transparent conductive oxides (TCOs), provides a versatile platform for high-performance all-optical switching and signal processing in optical networks.

1. INTRODUCTION

High-speed data transmission technology is increasingly required for embodied intelligence to leverage vast computational resources during real-time interactions with dynamic environments [1, 2]. However, this capability is currently constrained by the inherent limitations of traditional electronic communication. To address these limitations, all-optical modulators [3] have emerged as a versatile class of devices that operate through a range of physical processes such as carrier dynamics, excitonic effects, and phase transitions. Within this broad landscape, modulators based on optical nonlinearities, such as saturable absorption and the Kerr effect [4–6], have attracted considerable interest. Their inherently instantaneous light-matter interaction enables the manipulation of optical signals on femtosecond timescales, supporting data throughput far exceeding that of conventional electronic or carrier-based modulators. In these nonlinear processes, a switching beam transiently modifies the refractive index or absorption coefficient, providing a direct pathway for ultrafast all-optical signal processing.

To date, all-optical modulators have been experimentally validated across a diverse range of nonlinear materials. For instance, semiconductors such as silicon [7–9] remain the primary choice due to their mature fabrication processes, leading to extensive research and widespread adoption in integrated photonics. However, their inherently low nonlinear efficiencies necessitate complex structural designs to amplify light-matter interactions through resonant field enhancement; such designs include chains of silicon nano-antennas [7], Mie-type resonance nanoparticles [10], and nanostructured silicon membranes [11]. Meanwhile, lithium niobate ($LiNbO_3$), renowned for its strong optical nonlinearity [12, 13], has spurred extensive research into advanced modulators for supercontinuum generation [14], optical frequency combs [15], and four-wave mixing [16]. Despite these advantages, $LiNbO_3$ still faces fabrication challenges, such as etching difficulties that lead to non-vertical sidewalls, reduced device density, and integration hurdles with silicon photonics platforms [17].

Additionally, two-dimensional (2D) materials [10, 18], such as graphene and transition metal dichalcogenides (TMDs), have emerged as promising candidates for nonlinear photonicdevices. These materials support enhanced harmonic generation, enabling efficient and broadly tunable nonlinear optical responses spanning from visible to mid-infrared ranges. Recent advancements in 2D material-based modulators, including graphene-clad microfibers [19], graphene saturable absorbers [20], and WS_2 integrated with silicon-nitride waveguides [20], have paved the way for next-generation all-optical

* Corresponding authors: Hongsheng Chen (hansomchen@zju.edu.cn), Bingtao Gao (bgao@zju.edu.cn), Shilong Li (shilong.li@zju.edu.cn). † These authors contributed equally to this work.

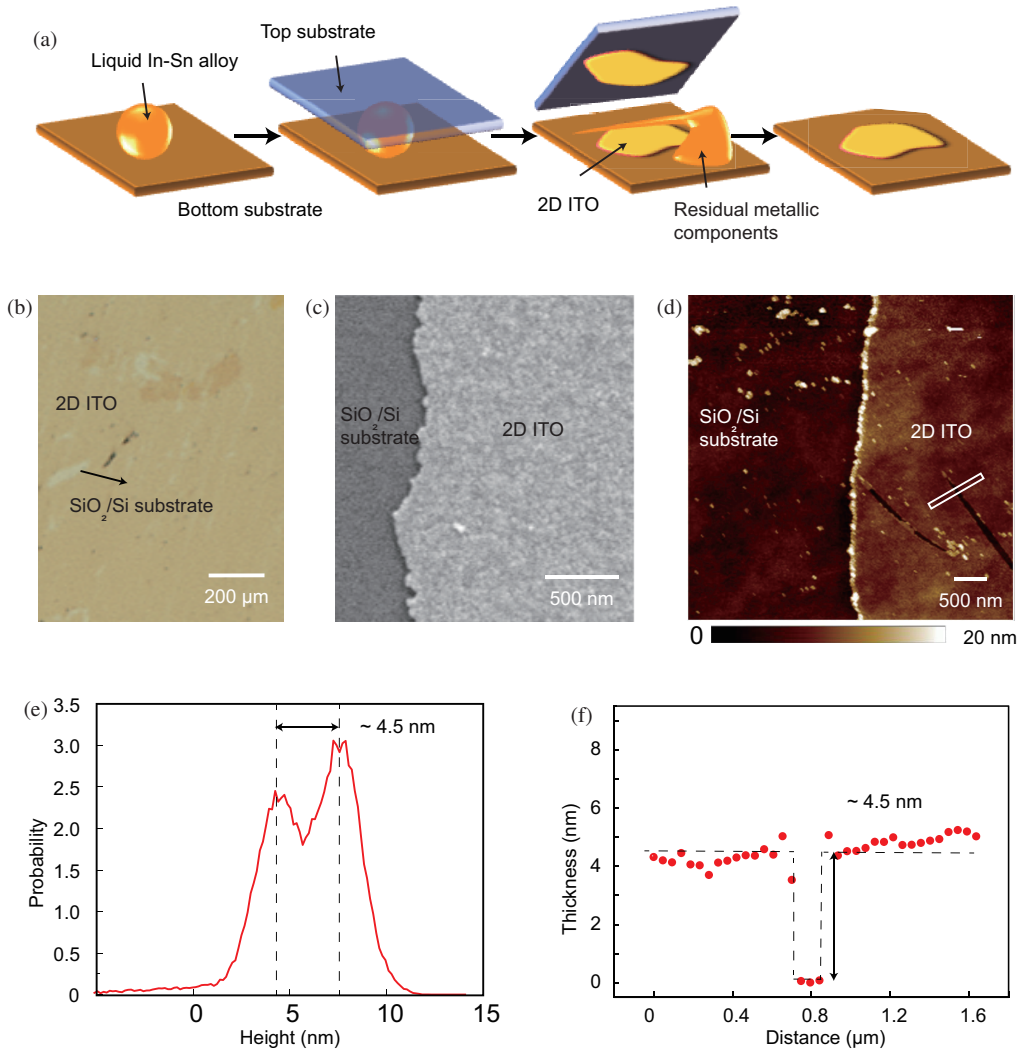

FIGURE 1. Fabrication and morphology of 2D ITO. (a) Schematic illustration of the synthesis process for 2D ITO samples. (b) Optical microscope images, (c) SEM images, and (d) AFM topographic maps of 2D ITO samples on a SiO_2/Si substrate. (e) Height distribution histogram and (f) linear thickness profile corresponding to the region indicated in (d), confirming a uniform thickness of ∼4.5 nm.

modulators suitable for high-speed space optical communication systems. However, practical applications are still hindered by the high optical absorption of graphene and the relatively complex synthesis of TMDs.

To address these challenges, transparent conductive oxides (TCOs) have emerged as a versatile material platform. In particular, 2D indium tin oxide (ITO) has garnered significant attention in nonlinear photonic devices due to its advantageous properties, including low optical losses, high electrical conductivity, and enhanced light-matter interactions facilitated by quantum confinement effects [21]. An exceptionally high second-order nonlinear susceptibility ($\chi^{(2)} \sim 1800$ pm/V) has been demonstrated in 2D ITO, surpassing that of traditional $LiNbO_3$ crystals by a factor of approximately 20. Despite this progress, a comprehensive understanding of its third-order nonlinear susceptibility $\chi^{(3)}$ remains elusive. As $\chi^{(3)}$ is the key parameter governing all-optical modulation schemes such as Kerr-based switching, saturable absorption, and four-wave mixing, its lack of characterization creates a critical disconnect between the material's proven capabilities and its practical implementations. This gap consequently hinders accurate modeling and performance prediction, severely limiting the development of efficient 2D ITO-based all-optical modulators.

In this work, we investigate the third-order nonlinear optical properties of 2D ITO, specifically focusing on the quantum-confinement phenomena that enable superior nonlinear efficiency within the 1550-nm telecommunications window. The atomically thin ITO films (∼4.5 nm) induce discrete electronic subband formation, which effectively intensifies the intersubband transition matrix elements and consequently augments the magnitude of $\chi^{(3)}$. Quantitative experimental characterization reveals an unprecedented $\chi^{(3)}$ value of 2×10^{-14} m^2/V^2, demonstrating a ∼300-fold enhancement relative to bulk ITO and a 5-fold improvement over graphene. The reported enhancement is primarily an intrinsic attribute of the 2D ITO quantum-well system, where quantum confinement modifies the electronic density of states to yield a distinct nonlinear identity. While the oblique-incidence configuration is employed

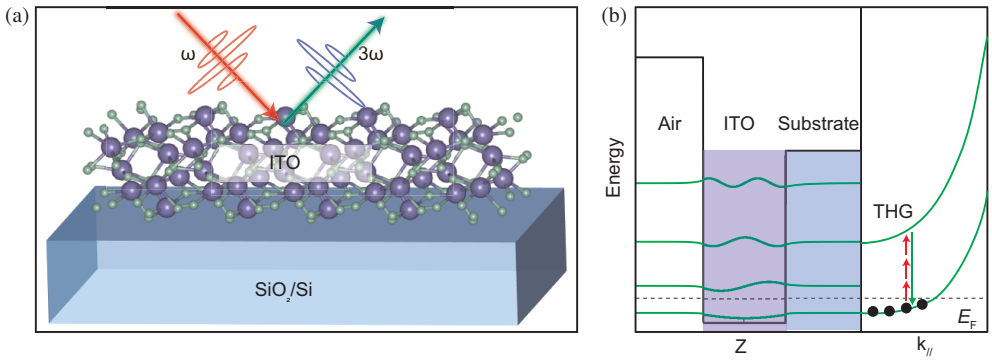

FIGURE 2. Atomic structure, electronic structure and quantum confinement in 2D ITO. (a) Schematic illustration of the 2D ITO film on a SiO_2/Si substrate in the van der Waals regime under optical excitation. (b) Electronic band diagram (left panel) overlaid with calculated subband wavefunctions, and subband dispersion (right panel) illustrating the intersubband transition pathways responsible for enhanced third-harmonic generation (THG). The electronic subband structure is obtained through theoretical calculations of the quantum-confined states, and the superimposed THG transition paths serve as a diagrammatic illustration of the nonlinear optical process.

to access the relevant perpendicular field component, the remarkable nonlinear response remains fundamentally rooted in the quantum-confined nature of the material. The synergy of enhanced nonlinear efficiency and maintained optical transparency establishes 2D ITO as a candidate material for ultracompact nonlinear photonic components.

2. RESULTS

2.1. Sample Fabrication and Characterization

To fabricate 2D ITO films, we employed a rapid printing method [22] utilizing a liquid In-Sn alloy, as illustrated in Figure 1(a). The alloy, composed of 95 wt% indium and 5 wt% tin, was prepared and melted by heating to 200°C. This temperature was optimized based on prior studies to enhance both the crystallization and electrical conductivity of the resulting films. Droplets of the molten alloy were pipetted onto preheated SiO_2 substrates — either thermally grown silicon dioxide or crystalline quartz — maintained at the same temperature to ensure uniform wetting. The liquid alloy underwent rapid oxidation via the self-limiting Cabrera-Mott mechanism [23], forming nanometer-scale oxide films within seconds. Subsequently, a second preheated substrate was pressed firmly onto the oxidized droplet, expelling excess liquid alloy laterally while maintaining the contact necessary for film formation. Careful separation of the substrates, with minimal horizontal shear, yielded ultrathin ITO films adhered to both surfaces via van der Waals forces. Residual metallic components were removed through an ethanol rinse, ensuring pristine oxide layers (see details in Methods). This fabrication process, illustrated in Figure 1(a), enables the scalable production of large-area, atomically thin ITO films tailored for nonlinear optical applications.

The morphology and uniformity of the fabricated 2D ITO films were assessed using optical and electron microscopy. An optical microscope image (Figure 1(b)) reveals a distinct contrast between the highly conductive ITO films and the dielectric SiO_2 substrate, confirming the presence of continuous, millimeter-scale films. The scanning electron microscopy (SEM) image (Figure 1(c)) further distinguishes the 2D ITO regions with a high clarity. For precise thickness determination, atomic force microscopy (AFM) was employed, as shown in Figures 1(d) and (f), respectively. Figure 1(d) presents an AFM topographic map, and the corresponding height distribution analysis in Figure 1(e) exhibits two distinct peaks — representing the substrate and the ITO film — with a separation of ∼4.5 nm. This measurement was corroborated by the height profile in Figure 1(f), which consistently indicates a film thickness of approximately 4.5 nm. In addition, the surface morphology of the printed 2D ITO films was evaluated, yielding a root-mean-square (RMS) roughness of approximately 0.8 nm. This exceptional level of surface uniformity, together with the structural continuity of the film, substantiates the effectiveness of the proposed rapid printing method for the realization of high-quality nonlinear optical platforms.

2.2. Principle of THG Enhancement in 2D ITO

As shown in Figure 2(a), the 2D ITO layer is placed on an SiO_2/Si substrate in the van der Waals regime, providing the structural basis for the quantum-confined electronic system considered here. The schematic also illustrates the optical excitation geometry associated with the nonlinear harmonic response. Figure 2(b) shows the electronic band diagram within the 2D ITO film. The film is sandwiched between air and an SiO_2/Si substrate, forming a quantum well that constrains the electron motion in the z-direction while allowing free in-plane movement. This quantum confinement leads to the discretization of energy levels and formation of discrete electronic subbands. The physical mechanism for the dramatic enhancement of third-order nonlinearities lies in the resonance effect between these quantized states. Specifically, when the incident photon energy matches the energy spacing between the subbands, the intersubband transitions are significantly amplified, creating a tailored energy landscape that maximizes light-matter interactions. This resonance mechanism fundamentally mirrors the principles underlying the previously reported enhancement of the second-order optical nonlinearity in 2D ITO [21].

To further quantify this enhancement and its symmetry properties, the third-order susceptibility $\chi^{(3)}$ can be derived based on the resonant density matrix formalism [24]:

$$\chi^{(3)}(\omega) = \frac{(N_{i-1} - N_i)}{\varepsilon_0 \hbar^3} \frac{e^4 z_{i-1,i} z_{i,i+1} z_{i+1,i+2} z_{i+2,i-1}}{[(\omega_{i+2,i-1} - 3\omega) - \mathrm{i}\Gamma_{i+2,i-1}][(\omega_{i+1,i-1} - 2\omega) - \mathrm{i}\Gamma_{i+1,i-1}][(\omega_{i,i-1} - \omega) - \mathrm{i}\Gamma_{i,i-1}]}. \quad (1)$$

Here, N, ε_0, and $\hbar$ represent the electron density, vacuum permittivity, and reduced Planck constant, respectively. The matrix element $z_{ij} = \langle i|\hat{z}|j\rangle$ represents the transition dipole length along the quantum-well direction, so that the corresponding dipole matrix element is $\mu_{ij} = -ez_{ij}$. The decay rate Γ_{ij} accounts for the linewidth or dephasing of the optical transition between subbands $|i\rangle$ and $|j\rangle$. These are associated with optically active subbands, which are crucial for understanding light-matter interactions. The transition frequency is defined as $\omega_{ij} = (E_i - E_j)/\hbar$, where E_i and E_j are the eigenenergies of the discrete subband states $|i\rangle$ and $|j\rangle$, respectively.

This expression highlights two critical insights. First, the dipole matrix elements involved in these transitions are on the order of $e \cdot d_{\text{well}}$, which is much larger than those in bulk materials, typically on the order of $e \cdot d_{\text{lattice}}$. Here, d_{lattice} and d_{well} denote the characteristic length scales of the lattice constant and quantum well thickness, respectively. Consequently, the third-order intersubband transition susceptibility can be enhanced by a factor of $(d_{\text{well}}/d_{\text{lattice}})^4$ compared with the corresponding bulk nonlinearity. For 2D ITO quantum wells, $d_{\text{well}}/d_{\text{lattice}} \approx 4.5$, resulting in theoretical enhancements of up to 410 for the third-order susceptibility, consistent with the order of magnitude observed in our experiments. Second, the formula dictates strict intersubband transition selection rules; specifically, only the longitudinal field component (z-direction) can trigger these transitions. Consequently, $\chi^{(3)}_{zzzz}$ (hereafter denoted as $\chi^{(3)}$) is the only non-vanishing component, which fundamentally governs the unique angular dependence of the nonlinear response observed in our experiments. Note that the depicted THG process is a coherent parametric process primarily mediated by virtual states, which exempts it from the strict parity selection rules that typically govern real transitions.

Using a self-consistent Poisson-Schrödinger solver for the 4.5 nm ITO quantum well, the calculated energy spacing between the quantized states matches the 1550 nm photon energy, satisfying the near-resonant condition. In addition, the intersubband transition linewidth in 2D transparent conducting oxides is broadened by carrier scattering, the resonant enhancement profile is relatively broad. Consequently, the $\chi^{(3)}$ is expected to maintain a consistently high magnitude across the telecom C-band (1530 to 1565 nm) without abrupt spectral degradation.

2.3. Experimental Nonlinear Optical Measurements

To bridge the gap between the theoretical predictions of $\chi^{(3)}$ and the practical material performance, we employed third-harmonic generation (THG) — a fundamental third-order nonlinear optical process — as a precise probe to characterize the nonlinear susceptibility of the 2D ITO quantum wells. The THG process, which involves the conversion of three fundamental photons into a single photon at triple the frequency, provides a direct and unambiguous measurement of the $\chi^{(3)}$ magnitude. The experimental setup used for these measurements is illustrated in Figure 3(a). A 1550-nm femtosecond laser, featuring a 150-fs pulse duration and a 100-MHz repetition rate, served as the fundamental pump source to excite the nonlinear response. The pump beam was reflected by a dichroic mirror and focused onto the 2D ITO sample through a 20× objective, while the generated THG signal was collected through the same dichroic mirror and recorded by a spectrometer coupled to an electron-multiplying charge-coupled device (EMCCD). Additionally, a flip mirror was utilized to redirect the optical path for in-situ imaging via a separate CCD camera, ensuring precise alignment and monitoring of the THG spots.

The power dependence of the THG signals from the 2D ITO sample, shown in Figure 3(b), follows a clear cubic power law, unequivocally confirming the third-order nature of the nonlinear process. This precise scaling not only aligns with the theoretical expectations for THG but also effectively rules out potential interference from lower-order nonlinearities or extraneous thermal artifacts. Figure 3(c) presents the THG spectra for different samples under p-polarized incidence at a 30° angle, with the inset displaying the corresponding THG emission spot from the 2D ITO sample. Remarkably, despite its atomic thickness (∼4.5 nm), the 2D ITO film generates THG signals approximately seven times stronger than those from a 300 nm bulk ITO film and exhibits a higher nonlinear conversion efficiency than a 700 nm $LiNbO_3$ crystal — a conventional benchmark in nonlinear optics.

2.4. Characterization of the Third-order Nonlinear Susceptibility

The calculation of $\chi^{(3)}$ from the measured THG intensity was based on the formula: $E_{\text{out}} = i\omega l/2nc \cdot \chi^{(3)} \cdot E^3_{\text{in}}$, where l denotes the light-matter interaction length. Given that the film thickness (4.5 nm) is significantly smaller than the coherence length in reflection, the nonlinear interaction occurs within the phase-matched regime, ensuring that phase mismatch is negligible. This allows for a direct, accurate extraction of $\chi^{(3)}$ based on the physical film thickness. In addition, n is the refractive index of ITO, c is the speed of light, and E_{out} and E_{in} represent the electric field amplitudes of the THG signal and fundamental pump, respectively. Crucially, due to z-axis subband quantization, intersubband selection rules limit dipole transitions strictly to out-of-plane polarization. This renders $\chi^{(3)}_{zzzz}$ the primary tensor component ($\chi^{(3)}_{zzzz} \gg \chi^{(3)}_{\text{in-plane}}$). Therefore, the nonlinear response is predominantly driven by the longitudinal electric field component (E_z). Since the magnitude of E_z is inherently coupled to the projection of the incident p-polarized beam, the measured $\chi^{(3)}$ exhibits a strong dependence on the incidence angle θ. Due to the finite numerical aperture of the objective lens, the maximum achievable incidence angle at the sample surface was limited to approximately 30°. As shown in Figure 4(a), experimental measurements reveal a representative

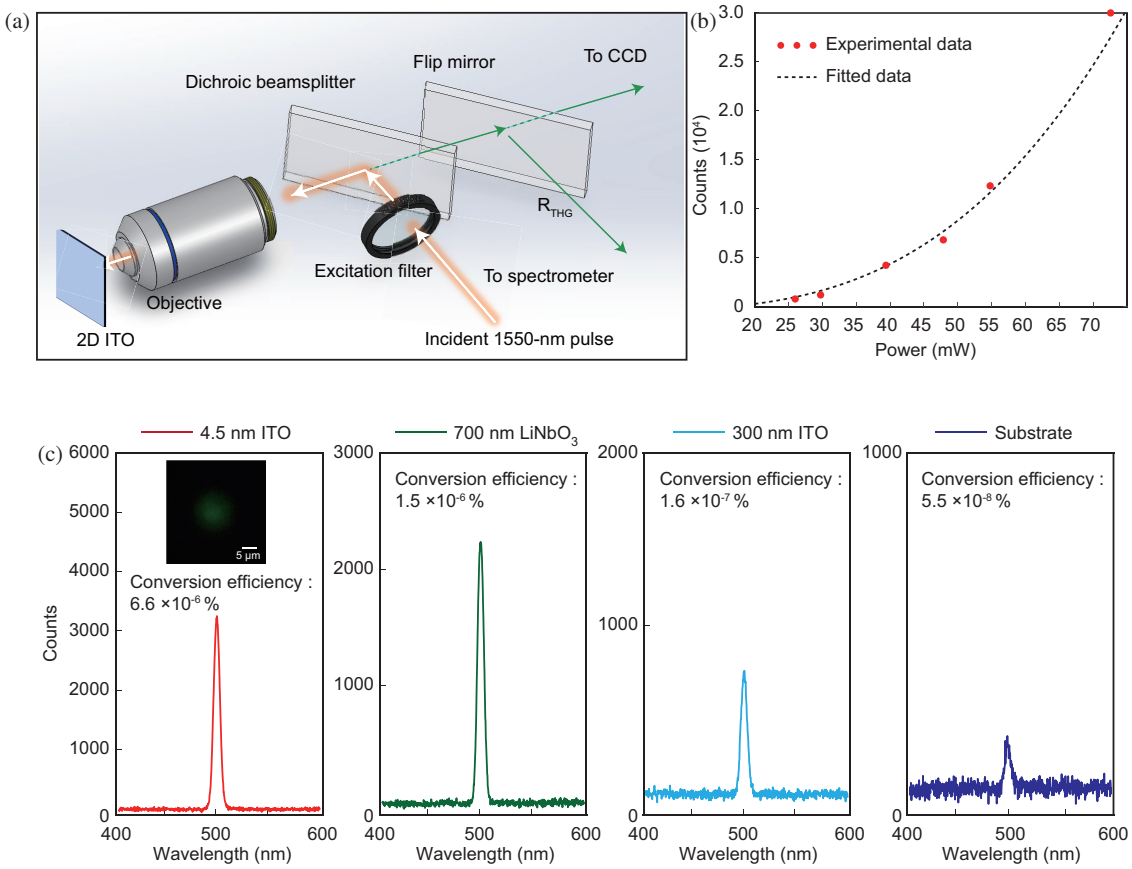

FIGURE 3. Nonlinear optical measurements of 2D ITO. (a) Schematic of the THG measurement setup. (b) THG signal counts as a function of incident laser power. The power-law fitted results confirm the expected cubic dependence on the incident power, thereby verifying that the observed signal originates from a third-order nonlinear process. (c) THG spectra of ∼4.5-nm 2D ITO, compared with 300-nm ITO, 700-nm $LiNbO_3$, and the substrate under 30° p-polarized incidence. Inset: Optical image of the THG spot. Note that, the comparisons were measured under the same excitation conditions — including identical pump wavelength (1550 nm), average excitation power (27 mW) and intensity (1.5 GW/cm^2). Also, the THG conversion efficiency ($\frac{I_{3\omega}}{I_\omega}$) is annotated alongside, where $I_{3\omega}$ is the generated third-harmonic intensity and I_ω is the incident intensity. In addition, statistical analysis of the extracted third-order nonlinear susceptibility $\chi^{(3)}$ yields a relative standard deviation (RSD $< 10\%$) across the measured 2D ITO regions.

angle-averaged $\chi^{(3)}$ value of 2.0×10^{-14} m^{2}V^2 (reaching up to 3.2×10^{-14} m^{2}V^2 at a 30° incidence angle). Furthermore, the experimentally measured $\chi^{(3)}$ follows a $\sin\theta$ trend [25], in excellent agreement with the theoretical predictions for intersubband transitions that rely on the longitudinal field component. This pronounced angular dependence provides compelling evidence for the quantum-confined nature of the enhanced nonlinearity in the 2D ITO structure, clearly distinguishing it from the isotropic response expected in bulk materials. It should be noted that while the $\chi^{(3)}$ values reported here are determined via THG measurements (corresponding to $\chi^{(3)}(3\omega;\omega,\omega,\omega)$), they provide a reliable benchmark for the material's nonlinear strength. Our intensity-dependent reflectivity measurements (Figure 4(b)) further confirm that this nonlinearity translates effectively to significant optical modulation at the fundamental frequency.

The systematic comparison presented in Figure 4(c) provides comprehensive insights into the third-order nonlinear merits of 2D ITO relative to other benchmark materials [26–32]. Quantitatively, the $\chi^{(3)}$ value of the 2D ITO demonstrates an approximately 300-fold enhancement over 300-nm bulk ITO films, as predicted by the theoretical scaling in Equation (1). The transition from quantum-confined to bulk-like nonlinear behavior was investigated, revealing that the prominent-subband signatures in our 4.5 nm films rapidly diminish as the thickness exceeds a certain threshold which is comparable to the de Broglie wavelength of electrons [33]. Furthermore, it outperforms the nonlinear responses of widely investigated 2D materials, including graphene and MoS_2, by more than a factor of five. Such a leap in material performance directly translates to improved metrics in nonlinear applications, such as all-optical modulators. This work thus establishes 2D ITO as a transformative candidate in nonlinear optics, paving the way for a new paradigm in designing ultra-compact and highly efficient functional devices for next-generation space optical communication.

To provide a rigorous evaluation of the practical performance of our platform, we have quantified its optical attenuation and evaluated comprehensive figures of merit (FOMs). Incorporating the established optical absorption coefficient for 2D ITO at

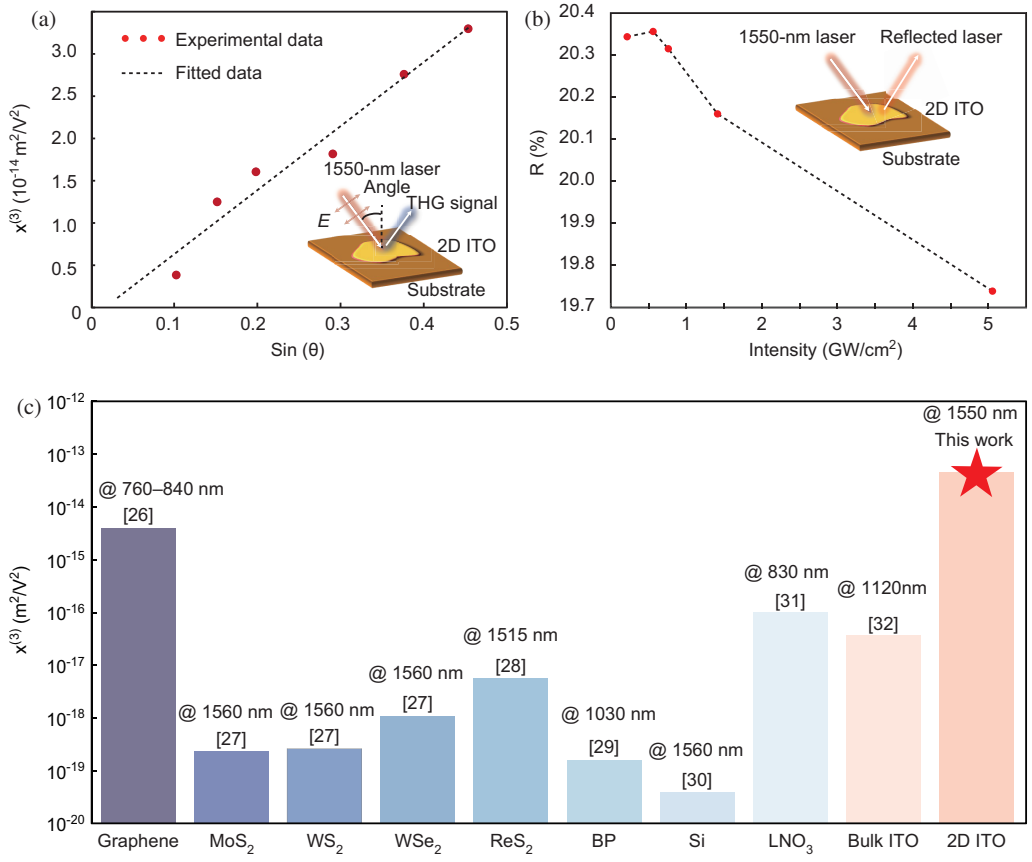

FIGURE 4. Nonlinear response characterization and $\chi^{(3)}$ comparison in 2D ITO. (a) Measured the effective $\chi^{(3)}$ as a function of sinθ. Here, θ is the incidence angle as indicated in the illustration, and the electric field possesses a component normal to the film plane that scales with sinθ. The dashed line corresponds to a linear fitting curve, providing compelling evidence for the role of the perpendicular electric field in the excitation mechanism. (b) Intensity-dependent reflectivity measurements of 2D ITO. (c) Comparison of $\chi^{(3)}$ values among various materials.

TABLE 1. Comparison of FOM.

Material	FOM	Working wavelength
Si	$7.1 \times 10^{-21}\,\mathrm{m^3/V^2}$	1560 nm
Graphene	$5.7 \times 10^{-22}\,\mathrm{m^3/V^2}$	760–860 nm
Bulk ITO	$4.3 \times 10^{-23}\,\mathrm{m^3/V^2}$	1120 nm
2D ITO	$2.0 \times 10^{-20}\,\mathrm{m^3/V^2}$	1550 nm

1550 nm ($\alpha = 1.6\times10^4\,\mathrm{cm^{-1}}$) [34], the figure of merit is determined to be FOM $= \chi^{(3)}/\alpha \approx 2.0 \times 10^{-20}\,\mathrm{m^3/V^2}$. A performance benchmark comparing 2D ITO against mainstream nonlinear materials is summarized in Table 1. As compiled in the table, while conventional integrated platforms such as silicon (Si) feature low linear optical loss, their $\chi^{(3)}$ values are orders of magnitude lower. Conversely, graphene provides a large $\chi^{(3)}$ but suffers from substantial optical absorption. Driven by quantum confinement, 2D ITO exhibits a high FOM, demonstrating a favorable trade-off between optical nonlinearity and absorption loss.

3. CONCLUSION

In conclusion, we have demonstrated a significant enhancement in the third-order nonlinear susceptibility of 2D ITO systems, validated through the THG effect. A record-high angle-averaged $\chi^{(3)}$ value of $2 \times 10^{-14}\,\mathrm{m^2/V^2}$ at the 1550-nm telecommunication wavelength has been realized, representing an approximately 300-fold improvement over 300-nm bulk ITO films and a 5-fold enhancement compared to graphene. This remarkable performance is attributed to the discretization of electronic states into subbands, which amplifies the intersubband transition strengths and enhances the light-matter interactions. These exceptional nonlinear properties, combined with maintained optical transparency, position 2D ITO as a promising material for developing compact, low-loss, and high-speed photonic modulators for next-generation AI-driven spatial optical communication systems.

ACKNOWLEDGEMENT

The work at Zhejiang University was sponsored by the National Natural Science Foundation of China (NSFC) under Grant Nos. 623B2092, 62405276, U25A20520, 62575258, and 62275231, as well as the Key Research and Development Program of the Ministry of Science and Technology under Grant Nos. 2022YFA1404704 and 2022YFA1405201. Y.U. Lee acknowledges support from the National Research Foundation of Korea (RS-2025-00521202) and the Korea Basic Science Institute (National Research Facilities and Equip-

ment Center) grant funded by the Korean government (MSIT) (No. RS-2024-00403036).

METHODS

Materials

Thermally grown SiO_2 (200 nm) on Si (100) and crystalline quartz (z-cut) substrates were acquired from Nanjing MK-NANO Tech. Co., Ltd.. High-purity metal particles, including indium (99.995% In) and tin (99.999% Sn), were sourced from SinoSantech Materials Tech. Co., Ltd. and used as received for the synthesis of the precursor alloy.

Cleaning procedure

Residual metal was removed from the substrates by first heating the samples to maintain the metal in a liquid state. The ITO surface was then meticulously cleaned using lint-free swabs soaked in ethanol. The efficacy of this procedure stems from the interfacial energetic difference: the ITO film is strongly bound to the substrate through van der Waals interactions, while the liquid metal exhibits preferential adhesion to the swab upon solidification — this process is accelerated by ethanol-induced evaporative cooling.

2D ITO characterizations

Themicrostructure of the 2D ITO films was characterized using a field emission SEM (Zeiss Sigma 300) operated at an accelerating voltage of 1 kV. AFM measurements were performed using a Bruker Dimension Icon system equipped with 'ScanAsyst-air' tips to obtain high-resolution topographic data. All AFM images were processed using the Gwyddion software package for thickness profiling, surface roughness analysis, and false-color rendering to enhance visualization.

DATA AVAILABILITY

The data that supports the plots within this paper and other findings of this study are available from the corresponding author upon reasonable request.

REFERENCES

[1] Li, J. and S. X. Yang, "Digital twins to embodied artificial intelligence: Review and perspective," *Intelligence & Robotics*, Vol. 5, No. 1, 202–227, 2025.

[2] Ficili, I., M. Giacobbe, G. Tricomi, and A. Puliafito, "From sensors to data intelligence: Leveraging IoT, cloud, and edge computing with AI," *Sensors*, Vol. 25, No. 6, 1763, 2025.

[3] Wu, Q., L. Peng, Z. Huang, X. Liu, M. Luo, D. Gao, and H. Meng, "Advancements in ultrafast photonics: Confluence of nonlinear optics and intelligent strategies," *Light: Science & Applications*, Vol. 14, No. 1, 97, 2025.

[4] Zhang, B., S. Ma, Q. He, J. Guo, Z. Jiao, and B. Wang, "Investigation on saturable absorbers based on nonlinear Kerr beam cleanup effect," *Optics Express*, Vol. 28, No. 5, 6367–6377, 2020.

[5] Ojaghi, S., S. Golmohammadi, and H. Soofi, "All-optical graphene-on-silicon slot waveguide modulator based on graphene's Kerr effect," *Applied Optics*, Vol. 60, No. 26, 7945–7954, 2021.

[6] Chatzidimitriou, D. and E. E. Kriezis, "Light propagation in nanophotonic waveguides considering graphene's saturable absorption," *Physical Review A*, Vol. 102, No. 5, 053512, 2020.

[7] Rahim, A., A. Hermans, B. Wohlfeil, D. Petousi, B. Kuyken, D. Van Thourhout, and R. G. Baets, "Taking silicon photonics modulators to a higher performance level: State-of-the-art and a review of new technologies," *Advanced Photonics*, Vol. 3, No. 2, 024003, 2021.

[8] Preble, S. F., Q. Xu, B. S. Schmidt, and M. Lipson, "Ultrafast all-optical modulation on a silicon chip," *Optics Letters*, Vol. 30, No. 21, 2891–2893, 2005.

[9] Cheng, Z., R. Cao, J. Guo, Y. Yao, K. Wei, S. Gao, Y. Wang, J. Dong, and H. Zhang, "Phosphorene-assisted silicon photonic modulator with fast response time," *Nanophotonics*, Vol. 9, No. 7, 1973–1979, 2020.

[10] Li, W., B. Chen, C. Meng, W. Fang, Y. Xiao, X. Li, Z. Hu, Y. Xu, L. Tong, H. Wang, *et al.*, "Ultrafast all-optical graphene modulator," *Nano Letters*, Vol. 14, No. 2, 955–959, 2014.

[11] Wu, R., J. Collins, D. Chekulaev, and A. Kaplan, "All-optical modulation and ultrafast switching in MWIR with subwavelength structured silicon," *Applied Sciences*, Vol. 9, No. 9, 1808, 2019.

[12] Hong, L., C. Hu, Y. Liu, H. He, L. Liu, Z. Wei, and Z.-Y. Li, "350–2500 nm supercontinuum white laser enabled by synergic high-harmonic generation and self-phase modulation," *PhotoniX*, Vol. 4, No. 1, 11, 2023.

[13] Zhu, X., F. Ni, H. Liu, J. Yu, F. Wang, Y. Cheng, X. Chen, and Y. Cai, "High-speed optical coherence manipulation based on lithium niobate films modulator," *PhotoniX*, Vol. 6, No. 1, 17, 2025.

[14] Lu, J., J. B. Surya, X. Liu, Y. Xu, and H. X. Tang, "Octave-spanning supercontinuum generation in nanoscale lithium niobate waveguides," *Optics Letters*, Vol. 44, No. 6, 1492–1495, 2019.

[15] Zhang, M., B. Buscaino, C. Wang, A. Shams-Ansari, C. Reimer, R. Zhu, J. M. Kahn, and M. Lončar, "Broadband electro-optic frequency comb generation in a lithium niobate microring resonator," *Nature*, Vol. 568, No. 7752, 373–377, 2019.

[16] Liu, S., Y. Zheng, Z. Fang, X. Ye, Y. Cheng, and X. Chen, "Effective four-wave mixing in the lithium niobate on insulator microdisk by cascading quadratic processes," *Optics Letters*, Vol. 44, No. 6, 1456–1459, 2019.

[17] Chen, G., N. Li, J. D. Ng, H.-L. Lin, Y. Zhou, Y. H. Fu, L. Y. T. Lee, Y. Yu, A.-Q. Liu, and A. J. Danner, "Advances in lithium niobate photonics: Development status and perspectives," *Advanced Photonics*, Vol. 4, No. 3, 034003, 2022.

[18] Chen, H., C. Wang, H. Ouyang, Y. Song, and T. Jiang, "All-optical modulation with 2D layered materials: Status and prospects," *Nanophotonics*, Vol. 9, No. 8, 2107–2124, 2020.

[19] Sun, F., L. Xia, C. Nie, J. Shen, Y. Zou, G. Cheng, H. Wu, Y. Zhang, D. Wei, S. Yin, and C. Du, "The all-optical modulator in dielectric-loaded waveguide with graphene-silicon heterojunction structure," *Nanotechnology*, Vol. 29, No. 13, 135201, 2018.

[20] Tasolamprou, A. C., A. D. Koulouklidis, C. Daskalaki, C. P. Mavidis, G. Kenanakis, G. Deligeorgis, Z. Viskadourakis, P. Kuzhir, S. Tzortzakis, M. Kafesaki, E. N. Economou, and C. M. Soukoulis, "Experimental demonstration of ultrafast THz modulation in a graphene-based thin film absorber through negative photoinduced conductivity," *ACS Photonics*, Vol. 6, No. 3, 720–727, 2019.

[21] Zhang, Y., B. Gao, D. Lepage, Y. Tong, P. Wang, W. Xia, J. Niu, Y. Feng, H. Chen, and H. Qian, "Large second-order susceptibil-

ity from a quantized indium tin oxide monolayer," *Nature Nanotechnology*, Vol. 19, No. 4, 463–470, 2024.

[22] Datta, R. S., N. Syed, A. Zavabeti, A. Jannat, M. Mohiuddin, M. Rokunuzzaman, B. Y. Zhang, M. A. Rahman, P. Atkin, K. A. Messalea, *et al.*, "Flexible two-dimensional indium tin oxide fabricated using a liquid metal printing technique," *Nature Electronics*, Vol. 3, No. 1, 51–58, 2020.

[23] Aukarasereenont, P., A. Goff, C. K. Nguyen, C. F. McConville, A. Elbourne, A. Zavabeti, and T. Daeneke, "Liquid metals: An ideal platform for the synthesis of two-dimensional materials," *Chemical Society Reviews*, Vol. 51, No. 4, 1253–1276, 2022.

[24] Boyd, R. W., A. L. Gaeta, and E. Giese, "Nonlinear optics," in *Springer Handbook of Atomic, Molecular, and Optical Physics*, 1097–1110, Springer, Cham, 2008.

[25] Li, S., H. Qian, and Z. Liu, "Anomalous nonlinear optical selection rules in metallic quantum wells," *Advanced Functional Materials*, Vol. 30, No. 21, 2000829, 2020.

[26] Hendry, E., P. J. Hale, J. Moger, A. K. Savchenko, and S. A. Mikhailov, "Coherent nonlinear optical response of graphene," *Physical Review Letters*, Vol. 105, No. 9, 097401, 2010.

[27] Autere, A., H. Jussila, A. Marini, J. R. M. Saavedra, Y. Dai, A. Säynätjoki, L. Karvonen, H. Yang, B. Amirsolaimani, R. A. Norwood, *et al.*, "Optical harmonic generation in monolayer group-VI transition metal dichalcogenides," *Physical Review B*, Vol. 98, No. 11, 115426, 2018.

[28] Cui, Q., R. A. Muniz, J. E. Sipe, and H. Zhao, "Strong and anisotropic third-harmonic generation in monolayer and multilayer ReS_2," *Physical Review B*, Vol. 95, No. 16, 165406, 2017.

[29] Yang, T., I. Abdelwahab, H. Lin, Y. Bao, S. J. R. Tan, S. Fraser, K. P. Loh, and B. Jia, "Anisotropic third-order nonlinearity in pristine and lithium hydride intercalated black phosphorus," *ACS Photonics*, Vol. 5, No. 12, 4969–4977, 2018.

[30] Kanemitsu, Y., S. Okamoto, and A. Mito, "Third-order nonlinear optical susceptibility and photoluminescence in porous silicon," *Physical Review B*, Vol. 52, No. 15, 10752, 1995.

[31] Wang, Q., S. Wang, W. Huang, Q. Gong, B. Yang, and J. Shi, "Ultrafast and large third-order optical nonlinearity of porous nanosized poly-crystal $LiNbO_3$ film," *Journal of Physics D: Applied Physics*, Vol. 35, No. 5, 430, 2002.

[32] Britton, W. A., F. Sgrignuoli, and L. D. Negro, "Structure-dependent optical nonlinearity of indium tin oxide," *Applied Physics Letters*, Vol. 120, No. 10, 101901, 2022.

[33] Wu, J., Y. Yang, Y. Qu, L. Jia, Y. Zhang, X. Xu, S. T. Chu, B. E. Little, R. Morandotti, B. Jia, and D. J. Moss, "2D layered graphene oxide films integrated with micro-ring resonators for enhanced nonlinear optics," *Small*, Vol. 16, No. 16, 1906563, 2020.

[34] Kondilis, A., E. Aperathitis, and M. Modreanu, "Derivation of the complex refractive index of ITO and ITON films in the infrared region of the spectrum by the analysis of optical measurements," *Thin Solid Films*, Vol. 516, No. 22, 8073–8076, 2008.